E JOURNAL

Benchmarking of plastic-based Additive Manufacturing Processes

Reindl, Thomas; Meisner, Dennis; Hierl, Stefan

Ostbayerische Technische Hochschule Regensburg, Technologie Campus Parsberg-Lupburg, Germany

https://doi.org/10.58134/fh-aachen-rte_2023_002

Abstract – *Additive Manufacturing (AM) is a future-oriented manufacturing technology that is experiencing an enormous boom in the times of Industry 4.0. As a result, various AM technologies and printer models from different manufacturers are entering the market over a short time span. With the advancing establishment of this manufacturing technology for series applications, the expectations and requirements of the fabricated components are also increasing. However, a major challenge is the application-specific selection of the most suitable AM process due to a lack of comparable data. Furthermore, there needs to be more know-how regarding the geometrical and mechanical characteristics of AM parts. This paper addresses this problem by comparing the three most common plastic-based AM processes in the areas of surface quality, dimensional accuracy, and mechanical properties. Roughness measurements, evaluation of a benchmark artifact, tensile tests, and load increase tests are carried out. Based on the results, the individual possibilities and limitations of the compared AM processes can be detected.*

Keywords – *Additive Manufacturing, benchmark artifact, dimensional accuracy, Fused Layer Modeling, mechanical properties, Multi Jet Fusion, process benchmark, Selective Laser Sintering, surface quality*

1. Introduction

Industry 4.0 is often declared as the latest industrial revolution in which advanced and intelligent production systems are established and promoted. Additive Manufacturing (AM) is an essential element of this industrial movement [1]. The technology is classified as future-oriented and attracts a lot of attention [2, 3]. Consequently, there is an increasing number of AM processes and printer types available on the market [4]. Furthermore, the expectations and demands towards additively manufactured components are rising due to the wide range of manufacturing options. This fact is also associated with the observed shift from prototyping to additive series production [5, 6].

Problematic is that there is hardly any comparable data for the many different AM processes. For this reason, selecting the most suitable printing process for the individual industrial manufacturing of functional components is much more challenging. Due to the increasing use of AM technology in the automotive, aerospace, and mechanical engineering sectors [6], mechanical properties are gaining importance, besides optical characteristics. This leads to the additional problem that, compared to conventional manufacturing methods, there is still a lack of know-how regarding the mechanical properties of AM components [7]. Therefore, this work aims to compare relevant AM processes according to different criteria. On the one hand, the lack of mechanical data will be addressed, and, on the other hand, a fundament for the process selection will be obtained.

A benchmark is defined and carried out to achieve the goals mentioned earlier in this work. Overall, the three different plastic-based AM procedures, Fused Layer Modeling (FLM), Multi Jet Fusion (MJF), and Selective Laser Sintering (SLS), are considered. This means that both the generally most used AM process (FLM) and the powder-based technologies most frequently used industrially in the field of polymers (SLS and MJF) are investigated in more detail [8]. The benchmark includes all the essential comparison criteria for functional components: surface quality, dimensional accuracy, and mechanical properties (static and dynamic load). The data are gathered by analyzing a self-constructed benchmark artifact and by performing roughness measurements, tensile and load increase tests. Finally, the results are compared to detect the individual strengths and weaknesses of the AM processes.

2. Methodology and Experiments

2.1 Printers, Materials, and Parameters

Before the benchmark methodology is described in more detail, the existing framework conditions must be considered. In this context, knowing which printer model, material, and manufacturing parameters represent the respective AM processes is essential. Since these factors significantly influence the properties of the printed components, the experimental results must also be strictly related to the underlying fabrication conditions. At least six test specimens are prepared for each printing process and orientation (see Figure 2-6) to ensure proper statistical reliability, as well as several benchmark parts in the most common building orientations (see Figure 2-3).

Typically industrially utilized printers and printing parameters are used for the process benchmark. For better comparability, materials based on polyamide 12 are selected for all three AM processes. Furthermore, the generation of the benchmarking data is carried out over several series of tests and an extended period. This led to a forced variation of the printer type for the data acquisition of the mechanical properties of MJF components. However, this aspect will be revisited in following subsections. A summary of these fundamentals is provided in the following Table 2-1.

Table 2-1: Manufacturing conditions for the process benchmark

AM process	FLM	MJF		SLS
printer type	Stratasys Fortus 380 mc	HP Jet Fusion 540	HP Jet Fusion 4200	EOS Formiga P110
material	Nylon 12	HP 3D High Reusability CB PA 12		PA 2200
support material	SR-110	–		–
refresh rate	–	20 %	25 %	40 %
layer height	0.254 mm (0.01") T16 nozzle	0.08 mm		0.10 mm
post processing	–	glass bead blasting		
further parameter details	[± 45°] infill pattern 2 outer contours	print mode: *cosmetic* (res.: 1200 dpi)	print mode: *mechanic* (res.: 1200 dpi)	EOS standard parameters beam-offset: 0.24 mm

2.2 Surface Quality

The surface quality achieved is the first quality indicator to be mentioned for component production. In previous studies, it was found that the measured surface roughness of additively manufactured parts depends on the printing orientation as well as on the printing parameters [9, 10]. Furthermore, different roughness heights (R_z) and mean waviness heights (R_a) are present according to the respective AM processes.

Roughness measurements after post-processing are carried out to investigate and compare the surface qualities achieved for the three selected plastic printing processes. Following DIN EN ISO 17296 [11], the tactile cutting method according to DIN EN ISO 4288 [12] is recommended for this purpose. The measurements are done using a MarSurf M 300 perthometer with MarSurf RD 18 from Mahr. Every single measuring value is composed of the measures of five partial sections. The measurements are done at critical component areas, respectively edge regions, as recommended by the standard (cf. [12]). Due to its simplicity and time efficiency, this testing method is frequently used in the manufacturing industry [13].

The roughness measurements are carried out using the specimens for the tensile tests. Since these are also printed in horizontal and vertical orientation, the effects of the up-skin, down-skin, and side-skin can be evaluated. The distinction between these three main surfaces is also found in comparable literature such as [14]. The print orientation of the tensile test specimens, surfaces considered, and measurement sections are shown in Figure 2-1.

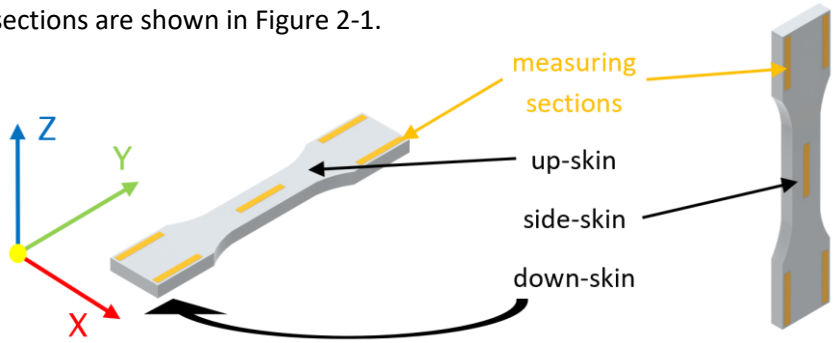

Figure 2-1: Roughness measurement positions (horizontal print orientation left, vertical print orientation right)

2.3 Shape, Position, and Dimensional Accuracy

Many different so-called benchmark artifacts have already been constructed and used to determine the capabilities and limitations of various AM processes in a comparable way [15 – 17]. However, no standardized artifact design is unrestrictedly suitable for a quantitative comparison regarding the dimensional accuracy of different AM procedures. Therefore, a separate benchmark geometry oriented to the proposals of DIN EN ISO/ASTM 52902 and VDI 3405 sheet 3.2 is used for the experiments [18, 19]. This artifact contains ten main characteristics, which can be used to consider the essential evaluation criteria. The designed benchmark part is shown in the following Figure 2-2.

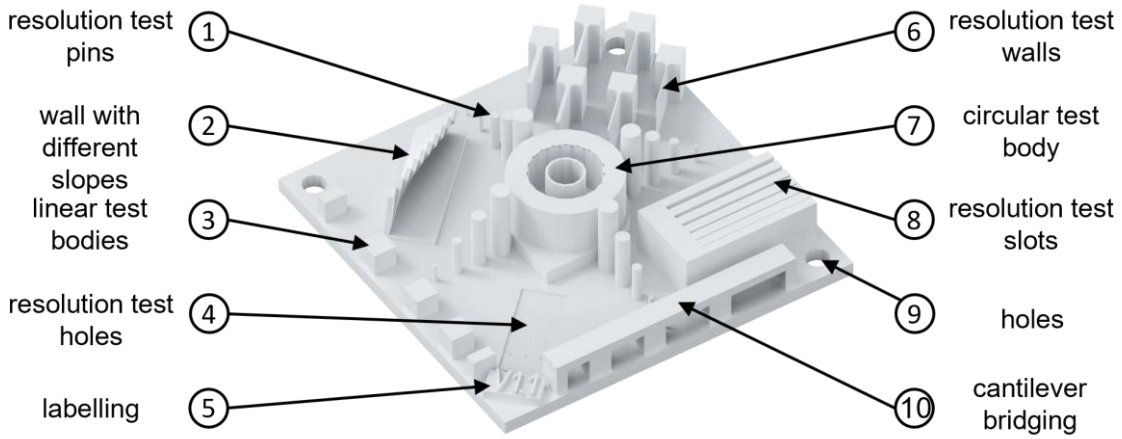

Figure 2-2: Overview of the benchmark artifact and the integrated features (80 mm x 80 mm x 3 mm base plate)

Using the benchmark artifact, the three central aspects geometric accuracy, resolution accuracy, and dimensional accuracy are considered. Starting with a closer look at the geometric accuracy, eight subcategories are evaluated. These are based on the definitions according to DIN EN ISO 1101 [20]. Which areas of the benchmark artifact are used to evaluate each of these categories is explained in the following.

- Both the existing deviations of the **straightness** and the **flatness** of the base plate are determined.
- The achieved **roundness** is evaluated at selected positions of the resolution test pins (1), the circular test body (7), and the holes (9).
- The existing deviations in terms of **parallelism** are measured by using the base plate and the features (3), (8), and (10).
- To evaluate the achieved **angularity** and **rectangularity**, selected positions of the base plate and the characteristics (2), base plate of (5), (7) and, (10) are investigated.
- The achieved accuracy regarding **concentricity** is determined based on the individual elements of the circular test body (7).
- The last category, **positional accuracy,** is examined for the locations of the holes (9) as well as for feature (7) in relation to the outer edges of the base plate.

The arithmetic mean values of all detected deviations within the respective accuracy categories are formed for the evaluation. Since the benchmark artifacts are produced in typical and several print orientations for each AM process, all measured values are averaged for each printing procedure for better comparability. The different printing alignments are shown in the following Figure 2-3.

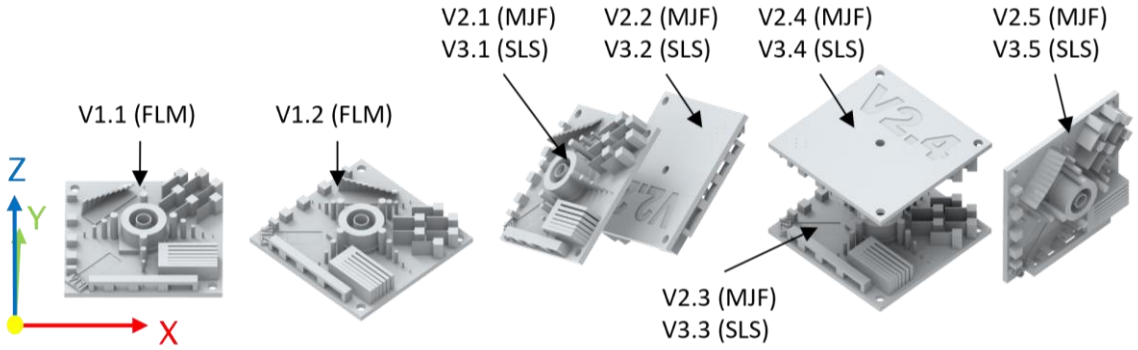

Figure 2-3: Print orientations of the benchmark artifacts for each AM process

The second essential investigation category covers resolution accuracy. Four different characteristics (see Figure 2-2) are used to determine the level of detail that can be produced by the respective AM processes and print orientations (see Figure 2-3). These include the following resolution features:

- test pins (feature 1): present four times, five cylinders with diameters of 0.5 – 4.0 mm
- test holes (feature 4): present three times, five holes with diameters of 0.1 – 0.5 mm
- test walls (feature 6): six walls with thicknesses of 0.1 – 1.0 mm
- test slots (feature 8): six slots with widths of 0.1 – 1.0 mm

A four-level system is introduced to evaluate the resolution accuracy:

- Very good print quality (tolerance class **m** according DIN EN ISO 2768-1 [21] is complied with; for dimensions < 0.5 mm, a tolerance of ± 0.05 mm is selected)
- Good print quality (fully printed feature)
- Poor print quality (feature is only partially or incorrectly printed)
- Very poor print quality (feature is not present or not recognizable)

In the evaluation, each benchmark part is considered separately. In the case of resolution features that are present more than once, such as feature (1) and (4), preference is given to the minimum print quality achieved. In addition, the color coding selected above is used for a simplified presentation (cf. Subchapter 3.2).

The size accuracy of the various benchmark artifacts is analyzed based on 18 defined individual dimensions. These are shown in Figure 2-4 below. Once again, the arithmetic mean value of the results of all benchmark parts per AM process is taken for better comparability. The dimensional deviations found are considered as absolute values.

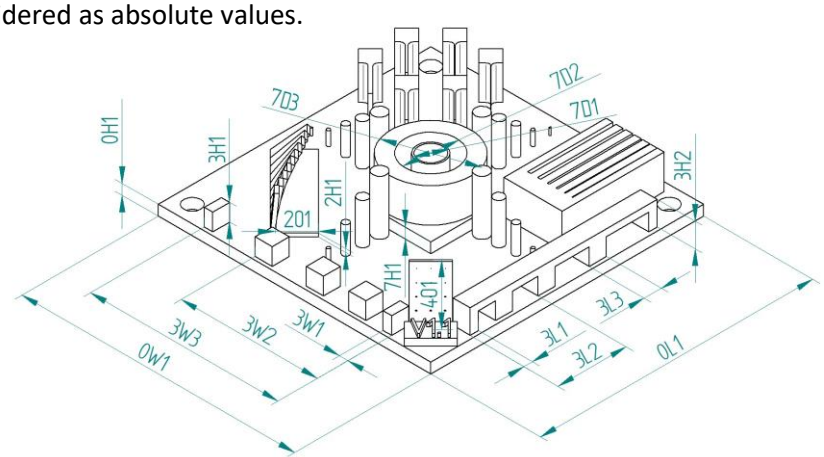

Figure 2-4: Measuring positions for testing the dimensional accuracy
(1. digit = feature number; w = width, l = length, h = height, o = oblique, d = diameter; 2. digit = sequential numbering)

2.4 Mechanical short-term Behavior

According to DIN EN ISO 17296 [11], the investigation of the mechanical short-time behavior for additively manufactured plastic components is recommended according to the test standard DIN EN ISO 527-2 [22]. However, the specimen geometries Type-1A and Type-1B presented in this norm have a high overall length, which is especially disadvantageous for vertically printed FLM parts. To improve printability and reduce printing time, SKZ (Süddeutsches Kunststoff-Zentrum) has developed a modified specimen geometry. The designed geometry is based on the Type-1A of DIN EN ISO 527-2 but has a shorter overall length and a shorter width of the sample shoulders and the narrow parallel section of the sample. The differences in tensile test data found due to the modified specimen geometry are considered unproblematic [23]. The geometry of the test specimens is shown in the following Figure 2-5.

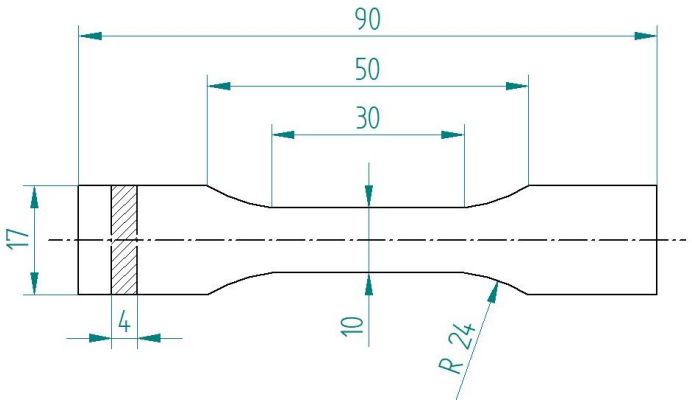

Figure 2-5: Tensile test specimen geometry Type-1A shortened with reference to [23]

The tensile tests are carried out with the Quasar 100 universal testing machine from Galdabini. It has a load cell with a maximum capacity of 5 kN and an extensometer MFX200 for strain measurement. Analogous to the already mentioned research report by SKZ, a test speed of 50 mm/min is used [23]. A high test speed increases the anisotropy effects. However, the stress values tend to be higher, while the strain values tend to be lower [23]. For the FLM specimens, the two standard print orientations, vertical (v) and horizontal (h), are considered. For the MJF and SLS parts, the experiments are extended by the two alignments oblique-horizontal (o-h) and oblique-vertical (o-v). The mentioned print orientations are shown in the following Figure 2-6.

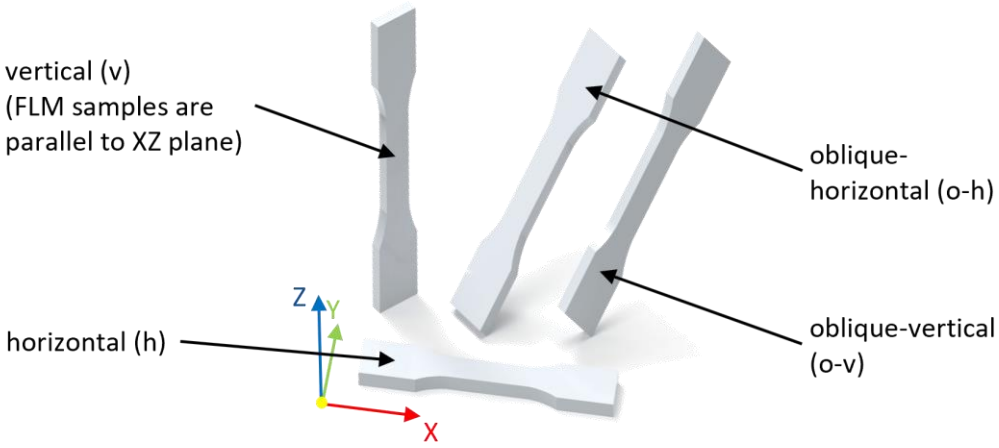

Figure 2-6: Print orientations of the tensile test specimens (powder application along x-axis)

2.5 Mechanical long-term Behavior

The analysis of the mechanical fatigue behavior is done with load increase tests, which are based on the hysteresis measurement method. With this experiment, findings regarding the dynamic load limits can be obtained after a comparatively short test duration [24]. Compared to the classical Wöhler test, this type of experiment offers an excellent compromise in terms of time efficiency and knowledge gain.

The analysis is carried out by performing force-controlled load-increase tests on a four-column testing machine from DYNA-MESS. In addition, the analogous specimen geometry and print orientations are used as for the tensile tests (cf. Subchapter 2.4). These are first subjected to a low, pulsating load at a constant frequency. The initial level is specified as a load level coupled mean load (σ_m). After a set amount of load cycles (N) is passed, σ_m is raised by a predefined load increase value ($\Delta\sigma$). The amplitudes are raised with each load increase, while the ratio (R) of the lower load level (σ_u) to the upper load level (σ_o) is kept constant across all load steps. The strain of the specimen is measured during the entire test duration.

It is essential to choose a sufficient amount of load cycles per load step as well as suitable values for σ_m and $\Delta\sigma$ to obtain reliable results. Generally, the fatigue strength is at a lower level than the tensile strength. In this way, it is possible to estimate in which load range failure will occur based on the results from the tensile test. The results of the tensile tests are discussed in more detail in subsection 3.3. Based on previous experiences as well as comparable research according to [24] and [25], the pulsating load is related to a constant ratio of R = 0.1. A center load of σ_m = 1 MPa is chosen as the initial load level. One load step contains a total of 1000 load cycles. In addition, a maximum of 25 load steps are run through during the experiment. The test frequency is set to 5 Hz. The stepwise increase of the center load is set to $\Delta\sigma$ = 1 MPa.

To determine the fatigue strength, the strain behavior across all the passed load cycles is considered. The values are determined in three steps, which are illustrated by an example in Figure 2-7 below. The onset of failure of the specimen is defined as the point of onset of plastic and thus nonlinear deformation. This point can be recognized by a sudden and over-proportional increase in the relative movement of the clamping jaws (corresponds to the strain curve). That nonlinear behavior can be seen most clearly in the load pauses during the changeover to the next load step (1). After that, the upper stress level (2) of the loading step before the damage onset is considered. The fatigue strength value (3) can then be read off from the secondary axis.

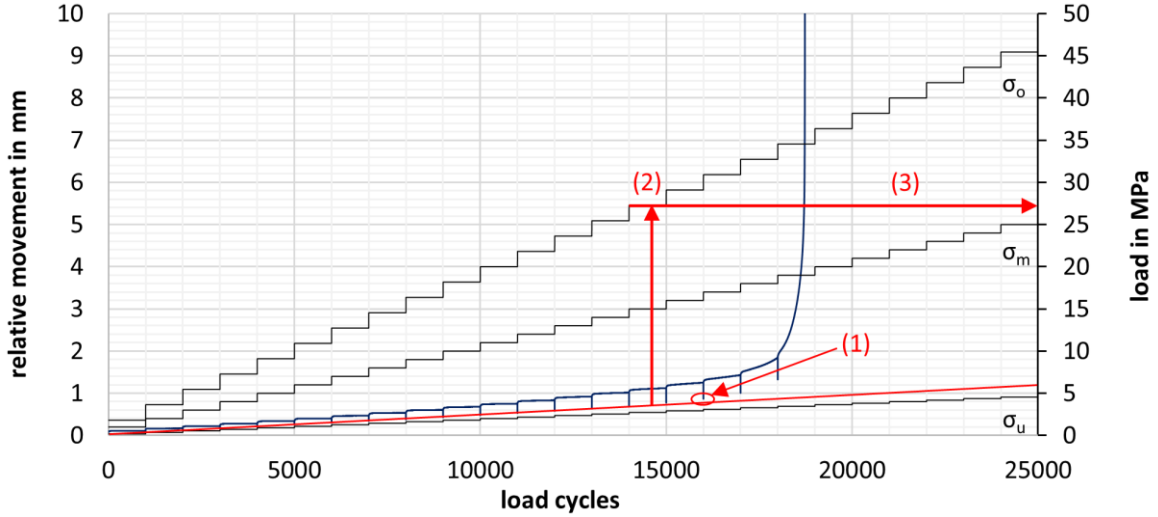

Figure 2-7: Schematic illustration of determining the fatigue strength

2.6 Conditioning

All test specimens and benchmark artifacts are conditioned before the tests are run. The climatic test chamber discovery DM 340 from ACS is used for conditioning according to DIN EN ISO 291 for a non-tropical environment at a temperature of 23 °C and relative humidity of 50 % for at least 88 hours [26].

3. Results and Discussion

In the following, the results are presented chronologically according to the preceding descriptions of the experiments. It should be noted that the results must be viewed critically since a representation of the selected AM processes is only feasible under the previously mentioned general conditions. Consequently, all findings must be related to the underlying representative conditions (cf. Table 2-1).

3.1 Surface Quality

The results of the roughness measurements show that the measured R_z and R_a values have a clear dependence on the considered surface and the respective AM process. In addition, it is noticeable that the differentiation into up-skin, side-skin, and down-skin shows the most significant influence for the FLM samples and the least for the SLS specimens. The comparisons of the measured roughness heights and mean waviness heights are shown below in Figure 3-1 and Figure 3-2. In addition, the standard deviations are included in the diagrams. In the context of surface quality, the MJF process is only represented by specimens of the HP Jet Fusion 540 printer.

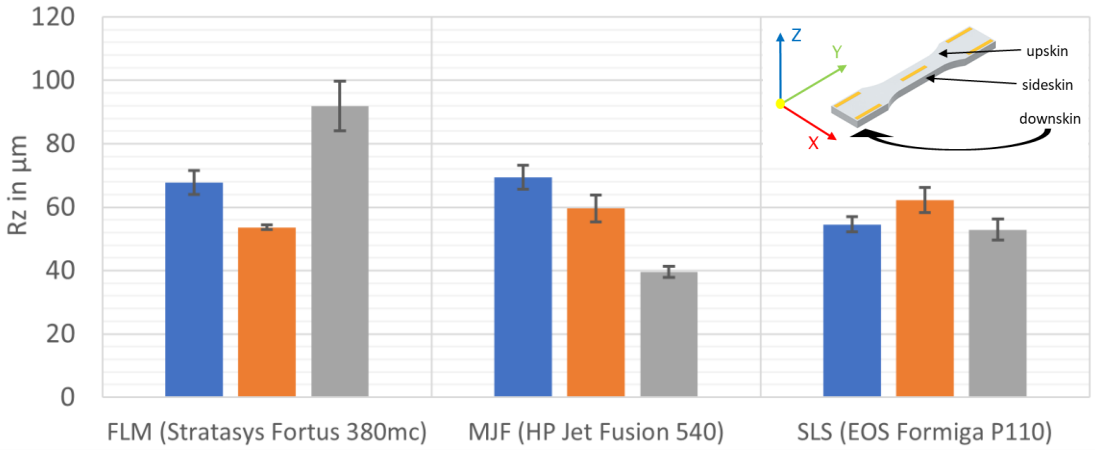

Figure 3-1: Roughness heights (blue = up-skin, orange = side-skin, grey = down-skin)

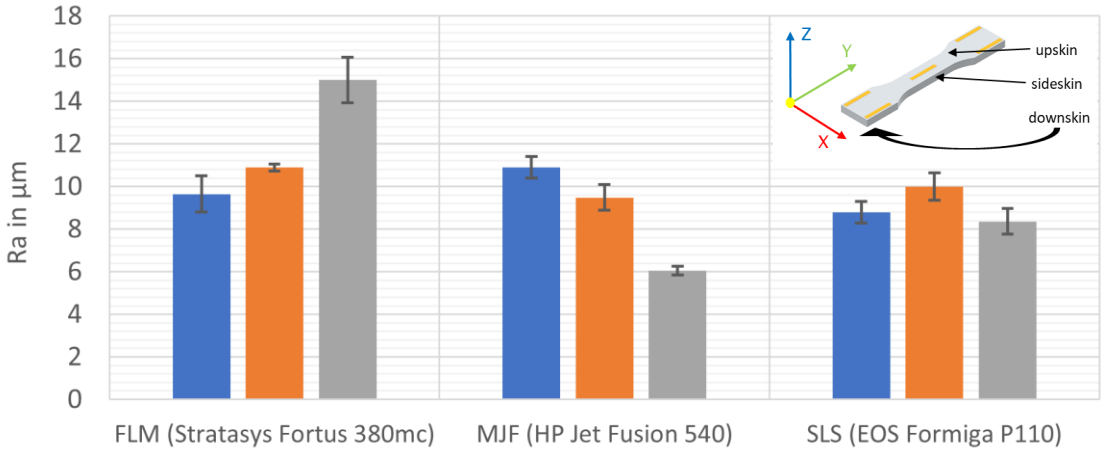

Figure 3-2: Mean waviness heights (blue = up-skin, orange = side-skin, grey = down-skin)

The evaluations of the surface measurements show that the R_a and R_z values for top-skin, side-skin, and down-skin differ most for the FLM specimens. This is directly related to the fact that with the Stratasys Fortus 380mc the first layer of the component is printed on support material. This leads to increased surface roughness. The up-skin and side-skin surfaces are not in contact with the support material and therefore have significantly better surface qualities. While the top-skin surface has higher roughness peaks, the average roughness of the side-skin surface is higher than that of the top-skin. The significant differences in surface quality depending on the print orientation of FLM components have also been demonstrated in comparable research [27, 28].

The surface measurements of the MJF parts show that the highest quality is achieved on the down-skin surfaces. The reasons for this are the process-specific surface defects observed during the investigations. These include both the surface sinking and the capillarity effect, which have a negative influence on the quality of the up-skin surfaces. For a more detailed description of these effects, it is referred to [29]. The measurements on the SLS test specimens show that the results hardly vary between up-, side- and down-skin.

Finally, it should be noted that the results obtained are to be limited only to the underlying test conditions. An individual improvement of the surface quality by parameter variation is possible for all three AM processes. Derived from these results, it is essential to consider the print orientation in correlation with the influences on the surface quality. Especially regarding the targeted additive series production, it is important to take these findings for visible and functional surfaces into account.

3.2 Shape, Position, and Dimensional Accuracy

Analogous to the chronological order in the second chapter, the evaluation regarding geometric accuracy is discussed first. For each of the eight considered categories, the absolute values of the dimensional deviations determined, averaged over all benchmark parts per AM process, are compared. The results are shown compactly in the following Figure 3-3. It should also be mentioned that in the context of dimensional accuracy, the MJF process is only represented by specimens of the HP Jet Fusion 540 printer.

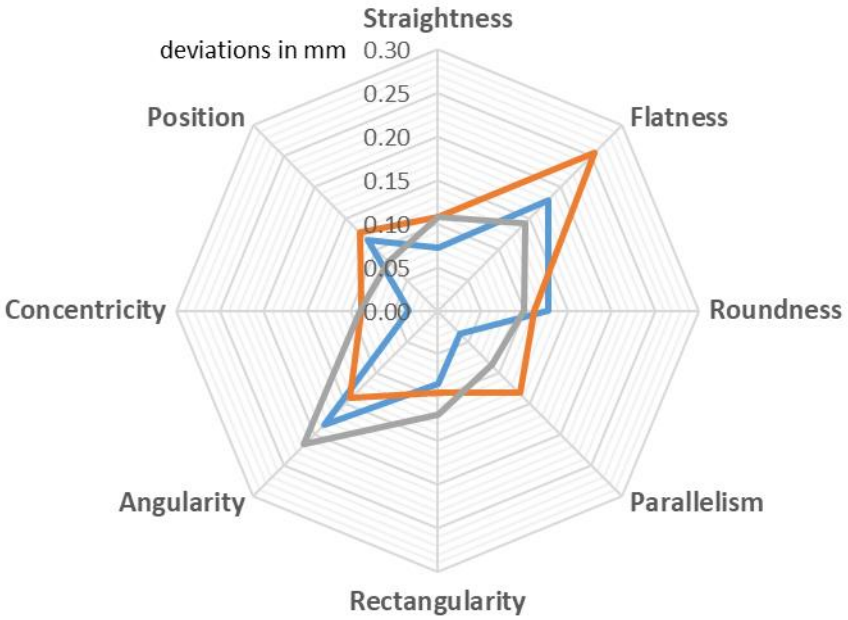

Figure 3-3: Achieved geometric accuracy (blue = FLM, orange = MJF, grey = SLS)

It can be seen that the FLM benchmark artifacts show the lowest deviations in four of the eight different categories. Only in the case of roundness do both MJF and SLS perform better. This weakness is primarily attributed to the printhead's limited positioning accuracy based on the printer's mechanical assembly [30]. In addition, in some cases, significant deviations of > 0.1 mm from the round shape can be observed at the joining seam.

The MJF benchmark parts show the largest deviations for parallelism, flatness, and position. Process typical surface imperfections cause this fact. The causes are primarily associated with the capillarity effect, surface sinking effect, or thermal bleeding [29]. Compared to the other two AM processes, the evident strength of the process is angularity.

SLS convinces in the categories of flatness, position, and roundness. The greatest inaccuracies are seen in angularity. In this respect, it should be noted that there is a systematic dimensional deviation for the SLS specimens during the tests. This will be discussed in detail in the following when considering the size accuracy. The reason for this deviation is that the shrinkage factor was not defined correctly. Among other things, this causes deviations in angularity.

Table 3-1 shows the results of the benchmark parts concerning the resolution characteristics. The color coding defined in the methodology section is used (cf. subsection 2.2). To emphasize the influence of the print orientation, no averaging of the results per AM process is done in this evaluation. Consequently, each benchmark part is considered separately.

Table 3-1: Resolution characteristics (dark green = very good print quality, light green = good print quality, orange = poor print quality, red = very poor print quality)

benchmark artifact / resolution feature	FLM		MJF					SLS				
	V1.1	V1.2	V2.1	V2.2	V2.3	V2.4	V2.5	V3.1	V3.2	V3.3	V3.4	V3.5
resolution test wall (1.0 mm)												
resolution test wall (0.8 mm)												
resolution test wall (0.6 mm)												
resolution test wall (0.4 mm)												
resolution test wall (0.2 mm)												
resolution test wall (0.1 mm)												
resolution test slot (1.0 mm)												
resolution test slot (0.8 mm)												
resolution test slot (0.6 mm)												
resolution test slot (0.4 mm)												
resolution test slot (0.2 mm)												
resolution test slot (0.1 mm)												
resolution test cylinder (4.0 mm)												
resolution test cylinder (3.0 mm)												
resolution test cylinder (2.0 mm)												
resolution test cylinder (1.0 mm)												
resolution test cylinder (0.5 mm)												
resolution test hole (0.5 mm)												
resolution test hole (0.4 mm)												
resolution test hole (0.3 mm)												
resolution test hole (0.2 mm)												
resolution test hole (0.1 mm)												

The evaluation clearly shows that both the AM process and the print orientation have a significant influence on the possible detail accuracy. The FLM benchmark parts show the best results overall for

the resolution test slots. This is mainly due to the fact that thermal bleeding led to poorer print quality for MJF and SLS. This effect cannot occur by using the powderless FLM process. Furthermore, there are only minor differences between the two FLM benchmark artifacts with different print orientations, which may also be due to statistical reasons.

The benchmark parts manufactured with MJF strongly depend on the print orientation. Thus, for example, the thermal bleeding effect can be reduced by adjusting the alignment in the build space. This thesis can be supported by the observations on benchmark artifact V2.5, which gives the best results for the resolution test slots and the resolution test holes for MJF. This is because heat build-up is reduced by having the primary orientation in the building direction and therefore, a printing pause between the layers in the slot areas is given.

The SLS benchmark parts' results also show a print orientation dependence. However, this is less significant than for the MJF parts. SLS shows the best results overall for the resolution test walls as well as for the resolution test cylinders. As indicated before, there is a slight discrepancy in the SLS test series concerning the shrinkage factor. This systematic oversize, in combination with the thermal bleeding effect, leads to very poor results for the resolution test slots and the resolution test holes. All in all, it should be noted that all results are to be related exclusively to the given framework conditions. In addition, no statements on scatter or statistical uncertainties are recorded since each benchmark artifact was produced only once.

Finally, the results for size accuracy of the considered widths (W), lengths (L), heights (H), diameters (D), and dimensions oblique (O) to the outer edges are shown in Figure 3-4.

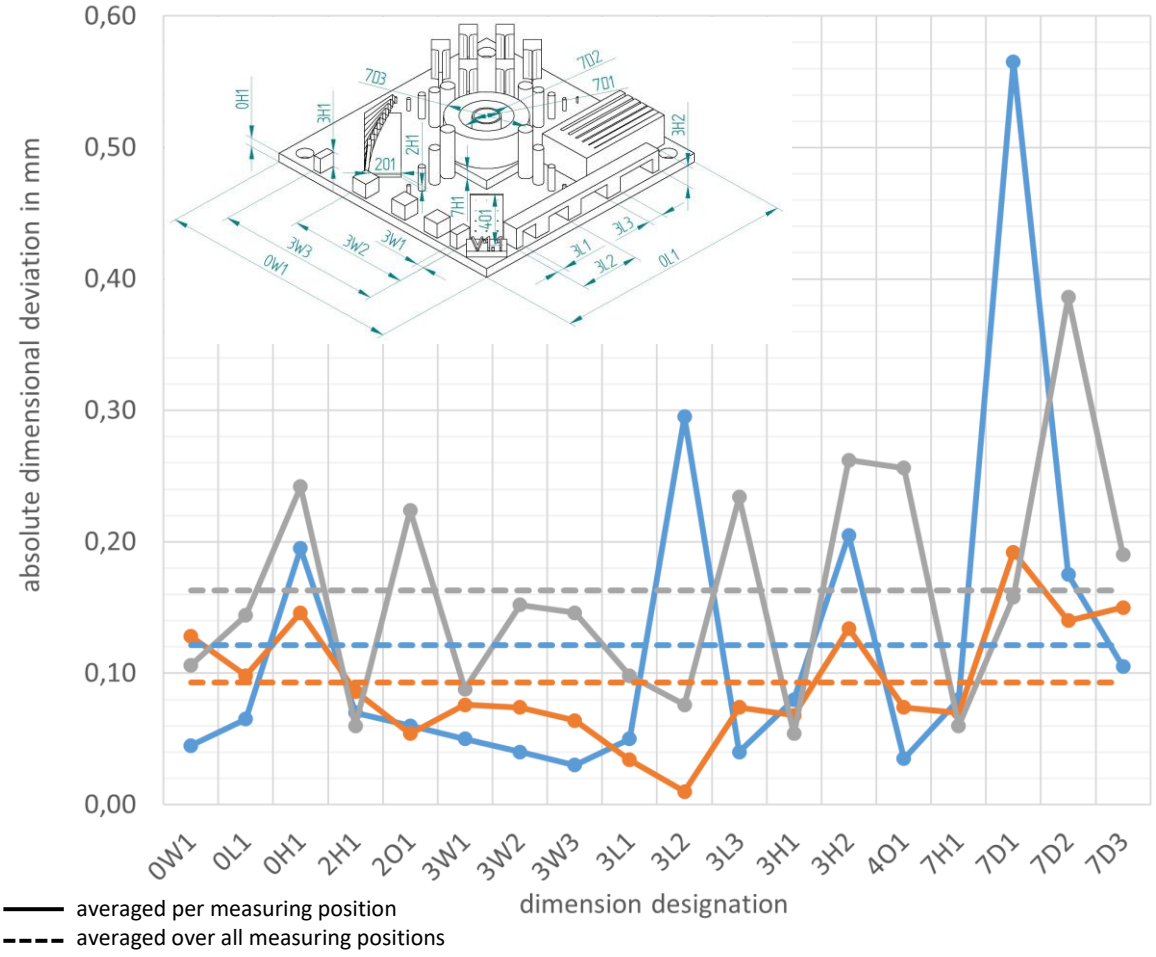

Figure 3-4: Dimensional accuracies (blue = FLM, orange = MJF, grey = SLS)

The averaged graphs per AM procedure of the dimensional deviations of the 18 different measurement positions allow an assessment of the respective dimensional accuracy. In total, MJF has no dimensional deviation of 0.2 mm or more at any measuring position. The results of the FLM benchmark parts are also primarily within this range, but three outliers clearly stick out. The highest outlier is a diameter at a thin-walled structure. This observation is in line with the finding that FLM shows the largest deviations in the roundness category compared to the other two procedures. The reasons for this have already been mentioned. As suspected, the dimensional deviations of the SLS components tend to be the highest. The reason for this is the aforementioned systematic error due to an insufficient definition of the shrinkage factor. Finally, it must be pointed out that the size accuracy depends on the AM process, print orientations, and individual print parameters. Consequently, the results can only be limited to the reference state. The accuracy achieved can be improved individually for each process by varying the manufacturing parameters like choosing a smaller nozzle diameter for FLM process to achieve a higher dimensional accuracy.

3.3 Mechanical short-term Behavior

As mentioned at the beginning, the raw materials used are as similar as possible to improve the comparability of the individual AM processes. In addition, the unique specimen cross-section is considered separately for each sample. Consequently, detected dimensional deviations cannot lead to a falsification of the results. Figure 3-5 shows the tensile strengths and tensile moduli determined. Since strain-based component dimensioning is also an alternative for plastics in producing functional components [31], the determined strains at tensile strength and at break are illustrated in Figure 3-6. In both figures, the identified standard deviations are displayed.

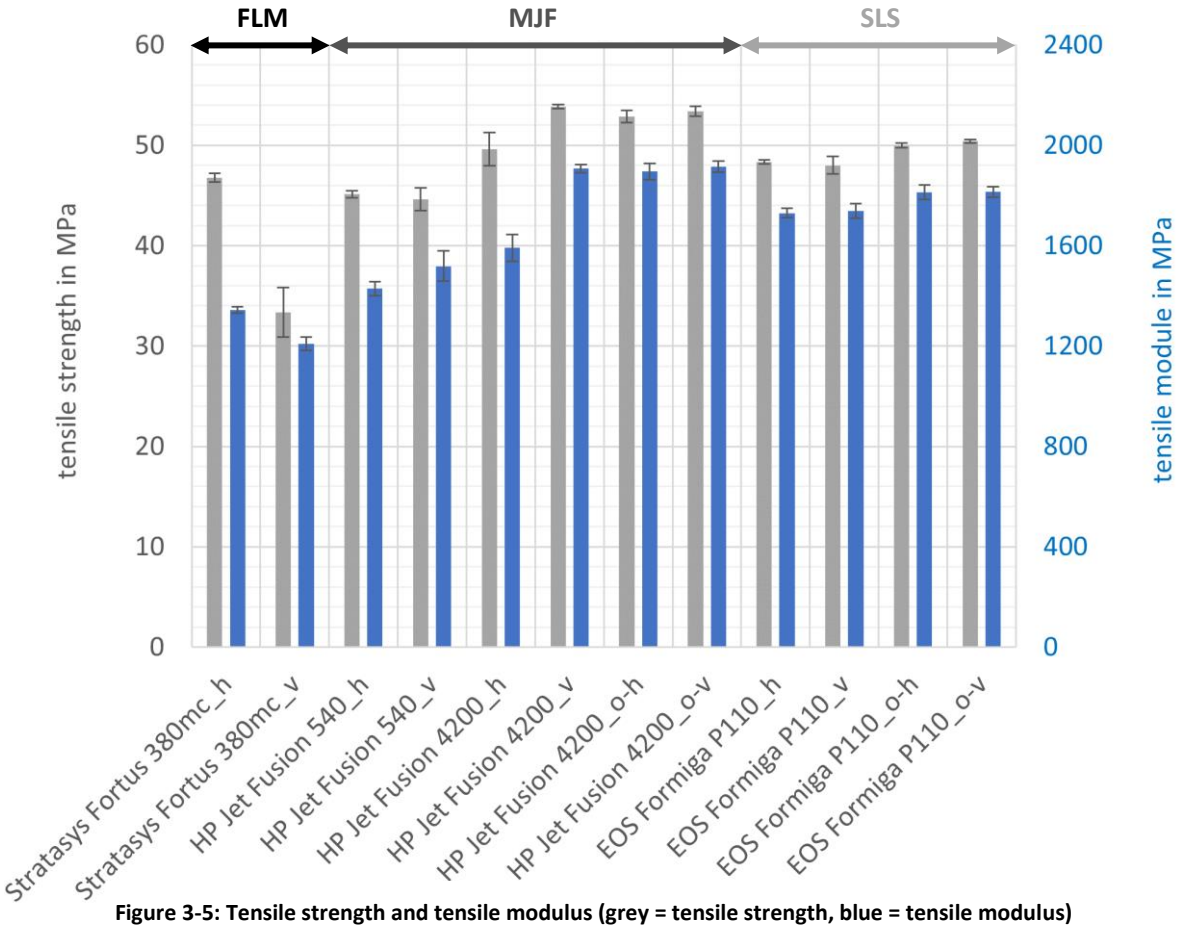

Figure 3-5: Tensile strength and tensile modulus (grey = tensile strength, blue = tensile modulus)

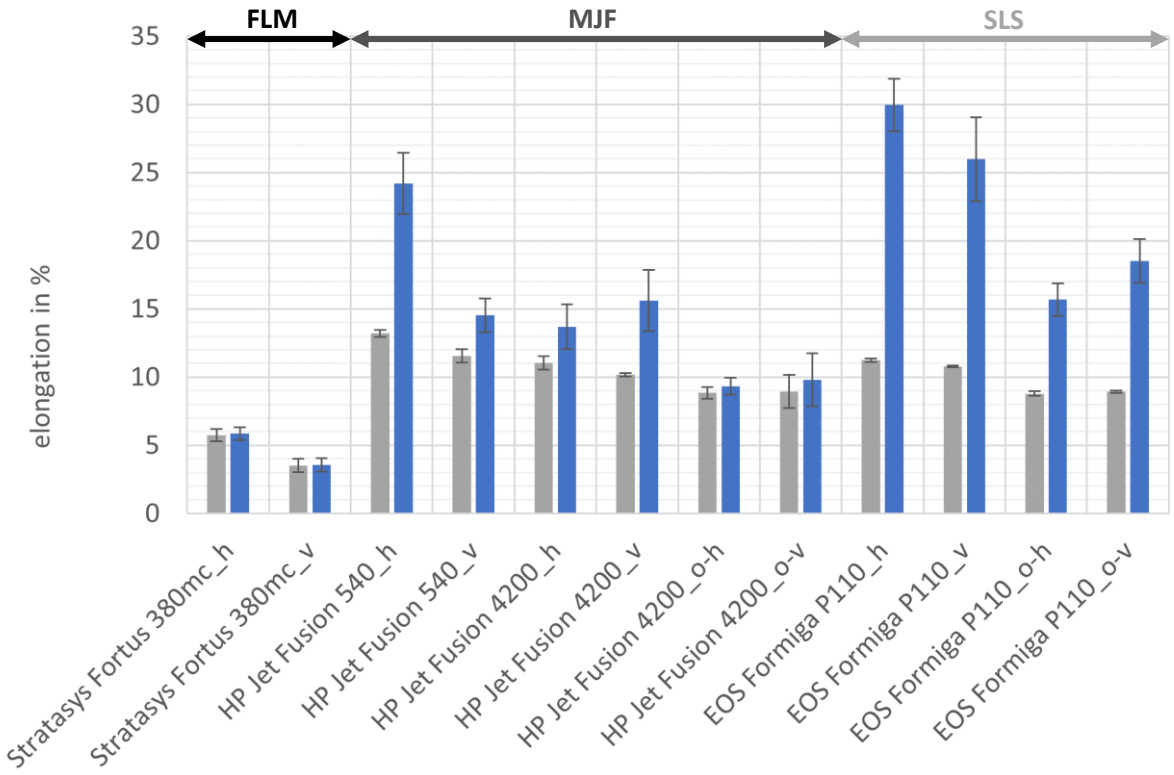

Figure 3-6: Elongation at tensile strength and elongation at break (grey = elongation at tensile strength, blue = elongation at break)

A closer look at the determined material properties reveals that the FLM process has the highest anisotropy. As already proven in various literature (e.g. [23, 32]), the horizontally produced FLM test specimens show significantly better mechanical properties than the vertically printed ones. The high process-related temperature gradient mainly causes the anisotropic behaviour of FLM components due to the layerwise extrusion principle. The decisive factor is the varying temperature gradients in the substructure of the components. If there is a large temperature difference between the solidified strands and the heated filament strand to be deposited, the bonding strength is poorer. In this context, polymer chain diffusion is an essential factor [33].

Comparing the results of the two MJF printers, it becomes apparent that there is a clear dependence on the printer model and the selected printing mode. This shows that the results cannot be generalized at all but must be limited to the given framework conditions. In addition, comparable research also concludes that the greatest strengths tend to be achieved with vertically printed test specimens [34]. In contrast, samples printed horizontally show the largest elongation values. The anisotropy effect is lower than with FLM.

Considering the results of the SLS specimens, a low directional dependence of the tensile strength and the tensile modulus is noticeable. This finding is consistent with comparable research work [34]. Compared to the other two AM methods, the SLS specimens tend to have the highest ductilities and, consequently, the maximum values for elongation at break.

The evaluation also shows that the assessment of the suitability of the AM methods for the individual application can be made based on the design strategy. This is because there is no uniform correlation between tensile strengths and the measured elongations. For example, the results of a strength-based

design strategy relying on the tensile strengths of the horizontally fabricated FLM and SLS specimens would provide comparable results due to the minor variation in their measured strength values. However, the identical specimens show clearly varying elongations. Consequently, applying a strain-based design strategy would result in significantly different component dimensioning for the FLM parts compared to the SLS parts. As a result, the choice of design strategy can lead to divergent results.

3.4 Mechanical long-term Behavior

In accordance with the procedure shown in Subchapter 2.5, the fatigue strength values are based on the upper stress values (σ_o), which are increased incrementally with each load step. For this reason, the fatigue strengths determined in the context of this investigation can only assume the values of these specified load levels. This can explain, on the one hand, the sometimes very large scatter and, on the other hand, the standard deviation of zero for the SLS parts manufactured in the horizontal position. The fatigue strengths determined are shown in the following Figure 3-7.

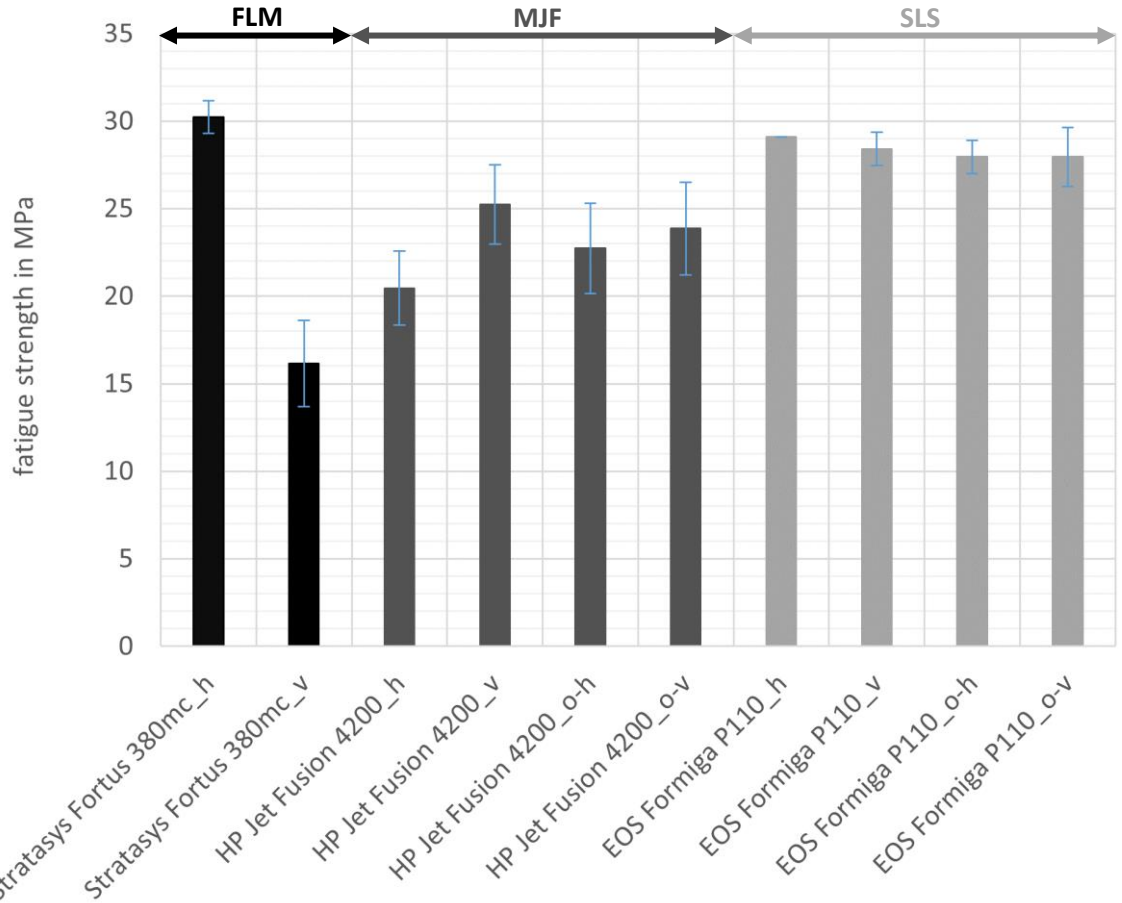

Figure 3-7: Fatigue strength (error bars of the EOS Formiga P110_h samples are zero due to the analysis methodology; cf. Subchapter 2.5)

In terms of the fatigue strengths determined, the FLM specimens again exhibit the greatest anisotropy. The reasons for this are analogous to those described for the mechanical short-term behavior (cf. Subchapter 3.3). However, it is noticeable that there is a varying correlation of the fatigue behavior to the determined short-term behavior depending on the AM process and print orientation.

In Table 3-2, a further overview is given to clarify the influence of the AM processes used and the respective printer type and print orientations considered. This shows the percentage values of the

fatigue strengths in relation to the short-term strengths determined. Since very similar raw materials are used, the influence of the individual AM processes can be seen.

Table 3-2: Ratios of short-term to long-term behaviors

	alignment	tensile strength	fatigue strength	ratio fatigue strength to tensile strength
FLM	h	46.8 ± 0.4 MPa	30.2 ± 0.2 MPa	65 %
	v	33.4 ± 2.5 MPa	16.1 ± 2.5 MPa	48 %
MJF	h	49.6 ± 1.7 MPa	20.5 ± 2.1 MPa	41 %
	v	53.9 ± 0.2 MPa	25.2 ± 2.3 MPa	47 %
	o-h	52.9 ± 0.6 MPa	22.7 ± 2.6 MPa	43 %
	o-v	53.4 ± 0.5 MPa	23.9 ± 2.6 MPa	45 %
SLS	h	48.3 ± 0.2 MPa	29.1 ± 0.0 MPa	60 %
	v	48.0 ± 0.9 MPa	28.4 ± 0.9 MPa	59 %
	o-h	50.0 ± 0.2 MPa	28.0 ± 0.9 MPa	56 %
	o-v	50.4 ± 0.2 MPa	28.0 ± 1.7 MPa	56 %

Considering the ratios, it can be seen that the fatigue strengths determined from the load increase test assume values in the range of approximately 40 – 65 % of the respective short-term strengths. The maximum fatigue strength was detected for the horizontally manufactured FLM specimens, whereas the vertically oriented FLM samples failed earliest. Again, the significant anisotropy of the FLM process can be seen. What is more surprising is that, despite the highest measured tensile strength values, the MJF specimens exhibit lower fatigue strengths than the SLS specimens. This trend is also evident from the calculated ratio values (MJF 41 – 47 % and SLS 56 – 60 %).

However, the fatigue strengths determined in the load increase test tend to have higher values compared to those from the Wöhler test, which is also evident in the literature, according to [35]. This phenomenon is due to the fact that in the classic Wöhler test, a higher load level is already present from the first cycle, which remains constant for the entire test duration.

4. Conclusion and Outlook

This research work addresses the problem of the lack of quantitative comparability and the lack of mechanical characteristic values for the three different AM processes (FLM, MJF, SLS). In the benchmarking process, results were determined in the comparative categories of surface quality, dimensional accuracy, and mechanical short-term as well as long-term behavior.

The roughness measurements showed that there are process-related differences between up-skin, side-skin, and down-skin surfaces. For the manufacturing of technically and optically relevant surfaces, the respective print orientation must therefore be considered individually for each AM process. In the field of dimensional accuracy, the AM procedures showed individual strengths and weaknesses. Again, there is a significant dependence on the selected print orientation as well as process-related influences. Furthermore, the significant influence of the AM process and the print orientation chosen on the mechanical short-term and long-term behavior was demonstrated. The ratios of fatigue to tensile strengths vary depending on the manufacturing process (FLM = 48 – 65 %, MJF = 41 – 47 %, SLS = 56 – 60 %).

The results of the process benchmark support the application-specific selection of the AM process. In addition, concrete values were determined, which can be used for the dimensioning of functional components. This database needs to be expanded in the future for more materials, printer types, and AM processes. This will further advance the establishment of AM in the industrial context.

Acknowledgement

We would like to thank IBL-HYDRONIC GmbH & Co. KG for providing and manufacturing test specimens and benchmark artifacts. Special thanks for the excellent cooperation go to the direct contact person Mr. Heindl. In addition, we would also like to thank the staff of the Technology Campus Cham for providing samples and the very good cooperation within this project. Special thanks to Ms. Jegel for the professional exchange and support.

Literature

[1] Dilberoglu, U. M.; Gharehpapagh, B.; Yaman, U.; Dolen, M.: The Role of Additive Manufacturing in the Era of Industry 4.0, In: Procedia Manufacturing, Vol. 11 (2017), pp. 545-554. DOI: https://doi.org/10.1016/j.promfg.2017.07.148.

[2] Saleh Alghamdi, S.; John, S.; Roy Choudhury, N.; Dutta, N. K.: Additive Manufacturing of Polymer Materials: Progress, Promise and Challenges, In: Polymers, Vol. 13 (2021), No. 5, 753. DOI: https://doi.org/10.3390/polym13050753.

[3] Neirinck, B.; Li, X., Hick, M.; Powder Deposition Systems Used in Powder Bed-Based Multimetal Additive Manufacturing, In: Accounts of Materials Research, Vol. 2 (2021), No. 6, pp 385-470. DOI: https://doi.org/10.1021/accountsmr.1c00030.

[4] Shah, J.; Snider, B.; Clarke, T.; Kozutsky, S.; Lacki, M., Hosseini, A.: Large-scale 3D printers for additive manufacturing: design considerations and challenges, In: The International Journal of Advanced Manufacturing Technology, Vol. 104 (2019), pp. 3679-3693. DOI: https://doi.org/10.1007/s00170-019-04074-6.

[5] Shahrubudin, N.; Lee, T. C.; Ramlan, R.: An Overview on 3D Printing Technology: Technological, Materials, and Applications, In: Procedia Manufacturing, Vol. 35 (2019), pp. 1286-1296. DOI: https://doi.org/10.1016/j.promfg.2019.06.089.

[6] Feldmann, C.; Schulz, C.; Fernströning, S: Digitale Geschäftsmodell-Innovationen mit 3D-Druck, Wiesbaden, Springer Fachmedien Wiesbaden, 2019.
DOI: https://doi.org/10.1007/978-3-658-25162-8.

[7] Bindl, S.; Csiky-Strauss, C.: Developing applications for additive manufacturing series production, In: 2017 IEEE European Technology and Engineering Management Summit (E-TEMS), 2017, pp. 1-7. DOI: https://doi.org/10.1109/E-TEMS.2017.8244220.

[8] Sculpteo: The State of 3D Printing 2021, retrieved in 12.2022: https://www.sculpteo.com/en/ebooks/state-of-3d-printing-report-2021/.

[9] Buj-Corral, I.; Domínguez-Fernández, A.; Durán-Llucià, R.: Influence of Print Orientation of Surface Roughness in Fused Deposition Modeling (FDM) Processes, In: Materials 2019, Vol. 12, No. 23, 3834. DOI: https://doi.org/10.3390/ma12233834.

[10] Rosso, S.; Meneghello, R.; Biasetto, L.; Grigolato, L.; Concheri, G., Savio, G.: In-depth comparison of polyamide 12 parts manufactured by Multi Jet Fusion and Selective Laser Sintering, In: Additive Manufacturing, Vol. 36, 2020, 101713.
DOI: https://doi.org/10.1016/j.addma.2020.101713.

[11] Additive Fertigung – Grundlagen – Teil 3: Haupteigenschaften und entsprechende Prüfverfahren (ISO 17296-3:2014); Deutsche Fassung EN ISO 17296-3:2016.

[12] Geometrische Produktspezifikation (GPS) – Oberflächenbeschaffenheit: Regeln und Verfahren für die Beurteilung der Oberflächenbeschaffenheit (ISO 4288:1996); Deutsche Fassung EN ISO 4288:1997.

[13] Launhardt, M.; Wörz, A.; Loderer, A.; Laumer, T.; Drummer, D.; Hausotte, T.; Schmidt,M.: Detecting surface roughness on SLS parts with various measuring techniques, In: Polymer Testing, Vol. 53, 2016, pp. 217-226.
DOI: https://doi.org/10.1016/j.polymertesting.2016.05.022.

[14] Kim, D. B.; Witherell, P.; Lu, Y.; Feng, S.: Toward a Digital Thread and Data Package for Metals-Additive Manufacturing, In: Smart Sustain Manuf Syst. 2017, Vol. 1, No. 1, pp. 75-99. DOI: https://doi.org/10.1520/SSMS20160003.

[15] Moylan, S.; Slotwinski, J.; Cooke, A.; Jurrens, K.; Donmez, M. A.: An Additive manufacturing Test Artifact. Journal of Research of the National Institute of Standards and Technology, Vol. 119, 2014, pp. 429-459.
DOI: https://doi.org/10.6028/jres.119.017.

[16] Vorkapic, N.; Pjevic, M., Popovic, M.; Slavkovic, N.; Zivanovic, S.: An additive manufacturing benchmark artifact and deviation measurement method, In: Journal of Mechanical Science and Technology, Vol. 34, 2020, pp. 3015-3026.
DOI: https://doi.org/10.1007/s12206-020-0633-2.

[17] Rebaioli, L.; Fassi, I.: A review on benchmark artifacts for evaluating the geometrical performance of additive manufacturing processes, In: The International Journal of Advanced Manufactruing Technology, Vol. 93, 2017, pp. 2571-2598.
DOI: https://doi.org/10.1007/s00170-017-0570-0.

[18] Additive Fertigung – Testkörper – Allgemeine Leitlinie für die Bewertung der geometrischen Leistung additiver Fertigungssysteme (AM-Systeme) (ISO/ASTM 52902:2019); Deutsche Fassung EN ISO/ASTM 52902:2019.

[19] Additive Fertigungsverfahren – Gestaltungsempfehlungen – Prüfkörper und Prüfmerkmale für limitierende Geometrieelemente, VDI 3405 Blatt 3.2 (2019-07-00).

[20] Geometrische Produktspezifikation (GPS) – Geometrische Tolerierung – Tolerierung von Form, Richtung, Ort und Lauf (ISO 1101:2017); Deutsche Fassung EN ISO 1101:2017.

[21] Allgemeintoleranzen – Toleranzen für Längen- und Winkelmaße ohne einzelne Toleranzeintragung; DIN ISO 2768-1:1991-06.

[22] Kunststoffe – Bestimmung der Zugeigenschaften – Teil 2: Prüfbedingungen für Form- und Extrusionsmassen (ISO 527-2:2012); Deutsche Fassung EN ISO 527-2:2012.

[23] Süddeutsches Kunststoff-Zentrum e.V. (Ed.), Mechanisches Langzeitverhalten additiv gefertigter Kunststoffbauteile, 1. edition, Herzogenrath, Shaker, 2018.

[24] Zilch-Bremer, H.: Realisierung des Hysteresis-Meßverfahrens, In: Hysteresis-Messverfahren – Das flexible Verfahren zur dynamischen Werkstoff- und Bauteilprüfung nach R. Renz (Ed. Ehrenstein, G. W.), 1993.

[25] Gassan, J., Bledzki, A. J.: Möglichkeiten zur Kontrolle der Festigkeit und Impactzähigkeit in naturfaserverstärkten Kunststoffen, In: Die Angewandte Makromolekulare Chemie, Vol. 272, No. 1, 1999, pp. 17-23. DOI: https://doi.org/10.1002/(SICI)1522-9505(19991201)272:1<17::AID-APMC17>3.0.CO;2-3.

[26] Kunststoffe – Normalklimate für Konditionierung und Prüfung (ISO 291:2008); Deutsche Fassung EN ISO 291:2008.

[27] Reddy, V.; Flys, O.; Chaparala, A.; Berrimi, C. E.; Amogh, V.; Rosen, B. G.: Study on surface texture of Fused Deposition Modeling, In: Procedia Manufacturing, Vol. 25, 2018, pp. 389-396. DOI: https://doi.org/10.1016/j.promfg.2018.06.108.

[28] Sagbas, B.; Durakbasa, N. M.: Profile and Areal Surface Characterization of Additive manufacturing Polymer and Metal Parts, In: Proceedings of the 12th International

Conference on Measurement and Quality Control – Cyber Physical Issue, 2019, pp. 240-246. DOI: https://doi.org/10.1007/978-3-030-18177-2_22.

[29] Mele, M.; Campana, G.; Monti, G. L.: Intelligent orientation of parts based on defect prediction in Multi Jet Fusion Process, In: Progress in Additive Manufacturing, Vol. 6, 2021, pp. 841-858. DOI: https://doi.org/10.1007/s40964-021-00199-x.

[30] Bakar, N. S. A.; Alkahari, M. R.; Boejang, H.: Analysis on fused deposition modelling performance, In: Journal of Zhejiang University-SCIENCE A, Vol. 11, 2010, pp. 972-977. DOI: https://doi.org/10.1631/jzus.A1001365.

[31] Kunz, J.: Reversibilität als Auslegungskriterium, In: Kunststoffe, 2018, No. 2, pp. 67-71.

[32] Gonabadi, H.; Yadav, A.; Bull, S. J.: The effect of precessing parameters on the mechanical characteristics of PLA produced by a 3D FFF printer, In: The International Journal of Advanced Manufacturing Technology, Vol. 111, 2020, pp. 695-709. DOI: https://doi.org/10.1007/s00170-020-06138-4.

[33] Bähr, F.: Methode zur modellierungsbasierten, präventiven Qualitätssicherung im Material Extrusion Verfahren, Universität Stuttgart (Ed.), 2020.
DOI: http://dx.doi.org/10.18419/opus-11326.

[34] Mehdipour, F.; Gebhardt, U.; Kästner, M.: Anisotropic and rate-dependent mechanical properties of 3D printed polyamide 12 – A comparison between selective laser sintering and multi jet fusion, In: Result in Materials, Vol. 11, 2021, 100213.
DOI: https://doi.org/10.1016/j.rinma.2021.100213.

[35] Ehrenstein, G. W.: Mit Kunststoffen konstruieren, 3. edition, München, Carl Hanser Verlag, 2020.

Contact

Thomas Reindl
OTH Regensburg, TC Parsberg-Lupburg
Am Campus 1
92331 Parsberg, Germany
Dennis Meisner
OTH Regensburg, TC Parsberg-Lupburg
Am Campus 1
92331 Parsberg, Germany

Prof. Dr.-Ing. Stefan Hierl
OTH Regensburg, TC Parsberg-Lupburg
Am Campus 1
92331 Parsberg, Germany
Email: **stefan.hierl@oth-regensburg.de**
WEB: **https://maschinenbau.oth-regensburg.de/labore/lasermaterialbearbeitung**